Proposal for detecting the π-shifted Cooper quartet supercurrent

Régis Mélin,[1,*] Romain Danneau,[2] and Clemens B. Winkelmann[1]
[1]*Univ. Grenoble-Alpes, CNRS, Grenoble INP, Institut NEEL, 38000 Grenoble, France*
[2]*Institute for Quantum Materials and Technologies, Karlsruhe Institute of Technology, Karlsruhe D-76021, Germany*

(Received 22 April 2023; accepted 11 July 2023; published 23 August 2023)

The multiterminal Josephson effect aroused considerable interest recently, in connection with theoretical and experimental evidence for correlations among Cooper pairs, that is, the so-called Cooper quartets. It was further predicted that the spectrum of Andreev bound states in such devices could host Weyl-point singularities. However, the relative phase between the Cooper pair and quartet supercurrents has not yet been addressed experimentally. Here, we propose an experiment involving four-terminal Josephson junctions with two independent orthogonal supercurrents, and calculate the critical current contours (CCCs) from a multiterminal Josephson junction circuit theory. We predict a generically π-shifted contribution of both the local or nonlocal second-order Josephson harmonics. Furthermore, we show that these lead to marked nonconvex shapes for the CCCs in zero magnetic field where the dissipative state reenters into the superconducting one. Eventually, we discuss distinctive features of the nonlocal Josephson processes in the CCCs. The experimental observation of the latter could allow providing firm evidence of the π-shifted Cooper quartet current-phase relation.

DOI: 10.1103/PhysRevResearch.5.033124

I. INTRODUCTION

Entanglement in electronic superconducting circuits is central to quantum engineering, and prototypes of quantum processors were recently realized, unveiling a variety of physical phenomena [1]. Entanglement engines were proposed in the early 2000s, with normal metal-superconductor-normal metal hybrids as sources of entangled Einstein-Podolsky-Rosen pairs of electrons [2–12]. A series of experiments addressed nonlocality in the DC current response [13–20] and quantum noise [21] as evidence for entangled split Cooper pairs [2–12]. On the other hand, the emerging field of all-superconducting multiterminal Josephson junctions [22–25] offers new perspectives, such as exotic transient quantum correlations among Cooper pairs, known as Cooper quartets [26–32]. Although a series of experiments reported clear signatures of Cooper quartets [33–36], these features were not observed by others [37–44], possibly due to delicate material and device fabrication issues. In parallel, multiterminal Josephson junctions also focused strong interest recently as a test bed of Floquet theory [45–52], as well as a platform for the emergence of energy level repulsion in Andreev molecules [53–59], the production of Weyl-point singularities in the Andreev spectrum [31,47,60–77], and the multiterminal superconducting diode effect [78,79].

Despite intense experimental efforts for observing signatures of the quartet state and its new physics beyond the standard resistively shunted Josephson junction model [33–35], novel schemes are necessary for ascertaining the Cooper quartets. When driving current between pairs of contacts in a multiterminal Josephson junction with an even number $2n$ of superconducting leads, n equations of current conservation are imposed by the external circuit. Those n constraints (for a total of $2n$ phase variables) allow for supercurrent inside a region in phase space parametrized by $2n - n \equiv n$ independent variables. With four terminals, a DC supercurrent is, thus, established within a two-dimensional region in the plane of the bias currents, separated from the resistive state by a one-dimensional critical current contour (CCC). In a recent work, Pankratova *et al.* [38] reported nonconvex shapes in the CCCs of four-terminal semiconductor-superconductor Josephson junctions. However, these nontrivial features appeared only at rather high magnetic fields, corresponding to about half a flux quantum threading the central part of the device. The observation of nonconvex CCCs was interpreted using random matrix theory, assuming time-reversal symmetry breaking, either due to an applied magnetic field or preexisting in the normal state [38].

Here, we demonstrate that in the presence of, at least, one contact with an intermediate transmission, another mechanism for the emergence of nonconvex CCCs is possible, which does not require a magnetic field. Namely, we find correspondence between the *quartet physics* and the emergence of nonconvex sharp-angled points in the CCCs at zero magnetic field. This distinctive signature stems from the interference between symmetric quartet channels, which are dephased by a transverse supercurrent (see Fig. 1). In other words, we demonstrate that *macroscopic* critical current measurements can probe the *microscopic* internal structure of entangled split Cooper pairs [2–9].

The article is organized as follows. The π-shifted quartets are introduced in Sec. II. The device and the model are

*regis.melin@neel.cnrs.fr

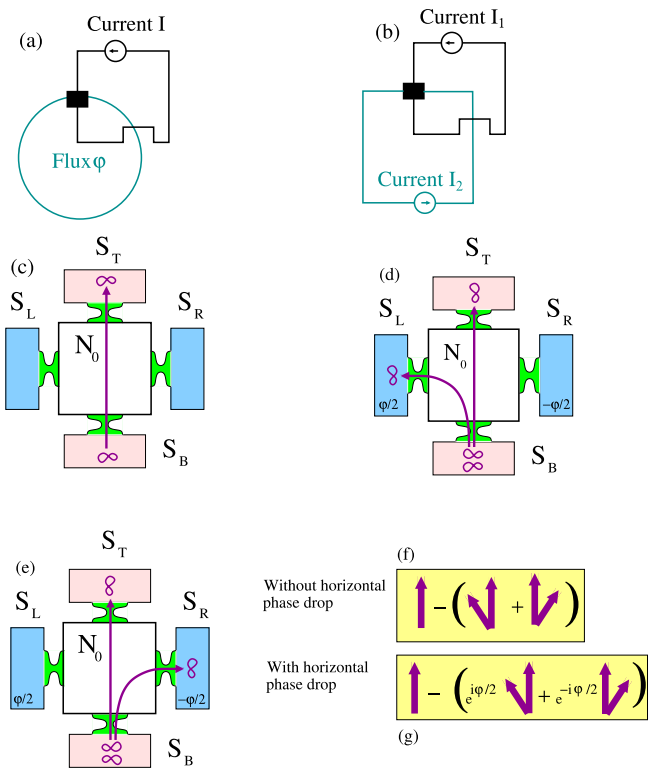

FIG. 1. Sketch of the superconducting four-terminal device with either one current and one phase bias (a) or two orthogonal current biases (b). The superconductors S_L, S_R, S_T, and S_B are connected to the normal metallic region N_0. The four N_0-S_i junctions consist of tunable quantum point contacts where the transmission of the N_0-S_T interface is reduced by a scaling factor τ_T. Panels [(c)–(e)] represent the lowest-order Josephson processes occurring in a simplified toy model. Panel (c) shows the two-terminal DC-Josephson effect from S_B to S_T, which is insensitive to the horizontal contacts. Panels (d) and (e) show the Cooper quartet processes, which take two Cooper pairs from S_B, exchange partners, and transmit the outgoing pairs into (S_T, S_L) and (S_T, S_R), respectively. In the presence of a horizontal phase drop, these two processes pick up opposite phases as shown in panels (f) and (g). This leads to interfering quartet supercurrent components within this simplified model, without and with horizontal phase drop, respectively. Due to the π shift, the critical current along the vertical direction in panel (f) is reduced by the two quartet processes. In panel (g), a phase drop along the horizontal direction dephases the negative contribution of both processes, resulting in an increased critical current and, thus, a nonconvex CCC.

presented in Sec. III. The numerical results, analytical and numerical, are presented and discussed in Sec. IV. Concluding remarks are provided in Sec. V.

II. π-SHIFTED COOPER QUARTETS

In this section, we provide physical arguments supporting the π-shifted Cooper quartet current-phase relation. The key underlying concept can readily be understood starting from a three-terminal configuration of Josephson junctions in the DC superconducting state, connecting the leads S with respective indices i, j, k [27,53] and biased with respective phases φ. The corresponding spin-singlet wave function of a split Cooper pair, for instance, between S_i and S_j takes the form

$$\psi = \frac{1}{\sqrt{2}}(c^+_{i,\uparrow}c^+_{j,\downarrow} - c^+_{i,\downarrow}c^+_{j,\uparrow}), \tag{1}$$

where $c^+_{i,\sigma}$ creates a spin-σ fermion in S_i. The splitting event in Eq. (1) can come along with a second one. The resulting composite four-fermion transient state, i.e., a Cooper quartet [27,33–36], ends up as two Cooper pairs transmitted into S_i and S_j, respectively, and described by

$$\langle\psi^2\rangle = -\langle c^+_{i,\uparrow}c^+_{i,\downarrow}\rangle\,\langle c^+_{j,\uparrow}c^+_{j,\downarrow}\rangle, \tag{2}$$

where $\langle\cdots\rangle$ is a quantum-mechanical expectation value (details can be found in Appendix A). By *probing the internal structure of (double) split Cooper pairs*, we mean providing experimental evidence for the negative sign in Eq. (2), which is a direct consequence of both quantum-mechanical exchange and the split Cooper pair structure of Eq. (1). Consequently, the relation between the quartet supercurrent I_q and the quartet phase φ_q is inverted

$$I_q(\varphi_q) = -|I^{c,q}|\sin\varphi_q \tag{3}$$

$$\varphi_q = \varphi_a + \varphi_b - 2\varphi_c, \tag{4}$$

where φ_a, φ_b and φ_c are the superconducting phase variables of the leads S_a, S_b and S_c respectively. Eq. (3) can be rewritten as $I_q(\varphi_q) = |I^{c,q}|\sin(\varphi_q + \pi)$ and this π shift is a macroscopic signature for the specific internal structure of single split Cooper pairs, see Eq. (1).

Another simple perspective on the π shift of the quartets readily follows from considering a single two-terminal superconducting weak link with normal-state transmission α. Here, the energy-phase relation can be Fourier-expanded as $E^J(\varphi) = E^J_0 + E^J_{2e}\cos\varphi + E^J_{4e}\cos 2\varphi + \cdots$. The $\cos\varphi$ term represents the Josephson Cooper-pair energy and is dominant in the limit of small transparency, whereas, the $\cos 2\varphi$ one describes correlated tunneling of two Cooper pairs. We find $E^J_{4e}/E^J_{2e} \approx -\alpha/16$ in the small-α limit and more generally $E^J_{4e}/E^J_{2e} < 0$ for all $\alpha < 1$, see Appendix B. This negative sign echoes the above current-phase relation of the quartets. More generally, our work proposes a method to directly reveal these π-shifted second-order Josephson harmonics, using a multiterminal configuration.

III. THE DEVICE AND MULTITERMINAL JOSEPHSON CIRCUIT THEORY

In this section, we present the two types of devices and the approximations sustaining multiterminal Josephson circuit theory. The proposed device consists of four BCS superconducting leads S_L, S_R, S_B, and S_T, with the respective superconducting phase variables φ_L, φ_R, φ_B, and φ_T, and connected via a square-shaped normal conductor N_0 as shown in Fig. 1. The external circuit imposes current in orthogonal directions, that is, a vertical current $I_v \equiv I_T = -I_B$ and a horizontal one $I_h \equiv I_R = -I_L$. The absence of coupling between I_v and I_h produces a square or rectangular CCC, whereas, rounded CCCs are indicative of coupling.

Our main result is that assuming a single or two contacts with transparency smaller than the others, nonconvex CCCs emerge in the (I_v, I_h) plane already under zero applied

magnetic field. We, thus, find reentrance of the dissipative state into the superconducting region as a distinctive signature of the π-shifted contribution of second-order Josephson harmonics. Furthermore, we show that the π-shifted Cooper quartet supercurrent produces distinctive reentrant sharp-angled points in the CCCs.

The four-terminal geometry is found by a straightforward generalization of Josephson circuits where now the I_v and I_h supercurrents result from an interference between multipair processes involving the phases of more than two terminals [27,30]. For instance, in a two-terminal Josephson junction, the terms corresponding to Cooper pairs transmitted from S_i to S_j couple to the difference $\delta_{i,j} = \varphi_i - \varphi_j$. Similarly, with four terminals, the relevant phase variables are then given by gauge-invariant combinations, such as $\delta_{i,j} + \delta_{k,l}$ [30], which reduces to Eq. (4) for three terminals [27].

In our multiterminal Josephson circuit model, we assume tunable contacts with a few transmission modes connecting the four superconductors to a central normal metal island (see Fig. 1), as was recently demonstrated in bilayer graphene-based two-terminal Josephson devices [80] and in multiterminal semiconducting-superconducting quantum point contacts [36]. Considering intermediate contact transparencies, although the DC-Josephson effect is dominant, the next-order Cooper quartets still yield a sizable contribution, whereas, the even higher-order terms are smaller. This *hierarchy* justifies the approach of the paper, considering within a single four-terminal device all the Josephson processes involving two, three, and then four terminals. The calculation involves two steps: our starting points are the approximate analytical expressions of the current-phase relations discussed above with sign and amplitude as free parameters. This allows comparing the CCCs with respectively positive or negative Cooper quartet contributions. From this we will arrive to the conclusion that nonconvex CCCs in zero field carry the unique signature of the microscopic π-shifted Cooper quartet current-phase relation and would be absent with a 0 shift.

We consider intermediate transparency interfaces, with hopping amplitudes J_L, J_R, J_B, and J_T connecting, respectively, the four superconducting leads S_L, S_R, S_B, and S_T to a normal tight-binding lattice N_0. The DC-Josephson supercurrent of Cooper pairs from lead S_i to lead S_j is written as $I_P = I_{i,j}^{c,P} \sin\,\delta_{i,j}$. The *nonlocal* DC-Josephson supercurrent of the Cooper quartets involves, at the lowest order in tunneling, the following three terms:

$$I_q = I_{i,j,(k)}^{c,q} \sin(\delta_{i,k} + \delta_{j,k}) + I_{i,(j),k}^{c,q} \sin(\delta_{i,j} + \delta_{k,j}) + I_{(i),j,k}^{c,q} \sin(\delta_{j,i} + \delta_{k,i}). \tag{5}$$

Here, $I_{i,j,(k)}^{c,q}$ for instance represents the critical quartet current of two pairs emitted by S_k and recombining into S_i and S_j. We introduce the individual channel transmissions τ_i such that all $J_i = \sqrt{\tau_i} J^{(0)}$ with $J^{(0)}$ a constant smaller than the bandwidth W. The critical currents scale as follows: $I_{i,j}^{c,P} = \tau_i \tau_j I_{i,j}^{c(0)}$ for the Cooper pairs, and $I_{i,j,(k)}^{c,q} = \tau_i \tau_j \tau_k^2 I_{i,j,(k)}^{c(0)}$, $I_{i,(j),k}^{c,q} = \tau_i \tau_j^2 \tau_k I_{i,(j),k}^{c(0)}$, and $I_{(i),j,k}^{c,q} = \tau_i^2 \tau_j \tau_k I_{(i),j,k}^{c(0)}$ for the Cooper quartets where the $I^{c(0)}$s do not scale with the transmissions.

IV. RESULTS

A. Polarization with one current and one phase bias

In this subsection, we present analytical results for the device polarized with one current and one phase bias, see Fig. 1(a). An external source drives a supercurrent from S_B to S_T and an external loop fixes the phase difference between S_L and S_R. We additionally assume that the N_0-S_T link has a tunneling amplitude J_T small compared to $J_L = J_R = J_B \equiv J^{(0)}$, i.e., $\tau_T \lesssim \tau_L$, τ_R, $\tau_B \lesssim 1$. Then, we make a perturbation expansion in tunneling of the Josephson circuit to the dominant order τ_T, neglecting the processes of order τ_T^2 (see Appendix C). In absence of the quartets, we find two types of processes: (i) The direct two-terminal DC-Josephson effect of the Cooper pairs from S_B to S_T [see Fig. 1(e)], and (ii) the two-terminal DC-Josephson processes of the Cooper pairs involving the lateral superconductors S_L and S_R. Adding now the quartets, we include all possible processes appearing on the orders of τ_T^0 and τ_T.

The cartoon shown in Fig. 1 illustrates the case where at the order of τ_T, the critical current I_v^c from S_B to S_T results from an interference between the amplitudes of the two-terminal DC Josephson effect and both Cooper quartets [see Figs. 1(f) and 1(g)]. Taking an opposite relative sign of the two- and three-terminal contributions, respectively, leads to a reduction of I_v^c upon including the Cooper quartets. Notably, because each quartet process picks up an opposite phase $\varphi_L = -\varphi_R \equiv -\varphi/2$, their respective contributions are dephased and the value of I_v^c is restored upon applying a supercurrent I_h (or a phase gradient) in the transverse direction as shown in Figs. 1(f) and 1(g).

Now, we evaluate the full set of microscopic two- and three-terminal processes at the relevant orders (details in Appendix C). Using the notations $\varphi_L = -\varphi_R = -\varphi/2$, we demonstrate in Appendix C that, at small τ_T and quartet Josephson energy $E_q = (\hbar/2e) I_q^c$, the critical current I_v^c from S_B to S_T can be approximated as

$$I_v^c \simeq \tau_T I_P^c \left\{ 3 + 6\frac{I_q^c}{I_P^c} - \frac{\varphi^2}{4}\left[1 + 14\frac{I_q^c}{I_P^c}\right]\right\}, \tag{6}$$

where I_P^c and I_q^c are proportional to the critical currents of the two- and three-terminal Cooper pair and Cooper quartet processes, respectively. Eventually, Eq. (6) predicts nonconvex CCCs if the condition,

$$I_q^c < -\frac{I_P^c}{14} \tag{7}$$

is fulfilled. In this case, the dissipative state reenters into the superconducting one, as a result of the π-shifted Cooper quartet current-phase relation coming from the spin-singlet minus signs in Eqs. (1) and (2).

We rewrite Eq. (6) as $I_v^c(\varphi) = \tau_T I_P^c F(\varphi/2\pi)$ with

$$F\left(\frac{\varphi}{2\pi}\right) = 3 + 6\frac{I_q^c}{I_P^c} - \pi^2\left(\frac{\varphi}{2\pi}\right)^2\left[1 + 14\frac{I_q^c}{I_P^c}\right]. \tag{8}$$

The variations of $F(\varphi/2\pi)$ are shown in Fig. 2, confirming emergence of nonconvex or convex CCC if $I_q^c < -I_P^c/14$ or $I_q^c > -I_P^c/14$, respectively.

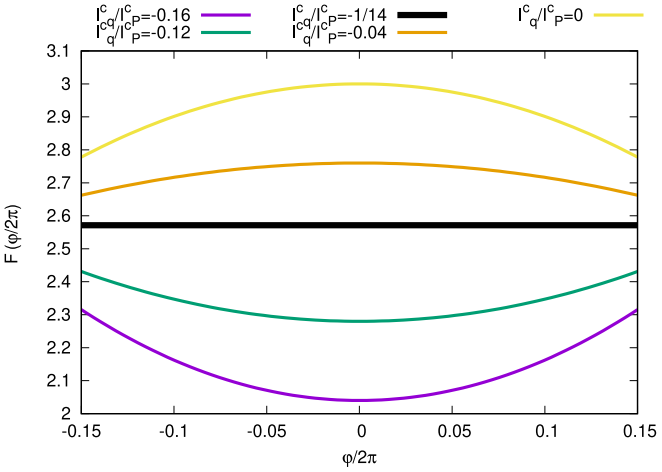

FIG. 2. The figure shows the shape of the CCC, i.e., $F(\varphi/2\pi)$ as a function of $\varphi/2\pi$, where $F(\varphi/2\pi)$ is proportional to the critical current, see Eq. (8). Polarization is with one current and one phase bias, see Fig. 1(a). The notation φ stands for the phase difference between the $N_0 - S_R$ and $N_0 - S_L$ contacts. Two regimes are obtained if $I_q^c < -I_P^c/14$ or $I_q^c > -I_P^c/14$, corresponding to nonconvex or convex CCCs, respectively.

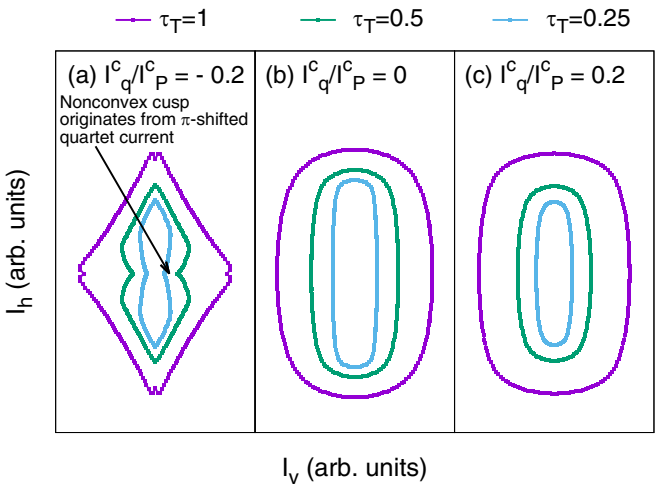

FIG. 3. Critical current contours in the (I_v, I_h) plane with $I_q^c/I_P^c = -0.2,\ 0,\ 0.2$ (in panels [(a),(c)], respectively) and with a single weak link. The contact transmission coefficients are such that $\tau_B = \tau_L = \tau_R = 1$ and $\tau_T = 1$ (magenta), $\tau_T = 0.5$ (green), and $\tau_T = 0.25$ (blue). Each panel is rescaled to full size on the I_v and I_h axes. Polarization is with two orthogonal current biases, see Fig. 1(b). Temperature is set to zero.

B. Polarization with two orthogonal current biases

In this subsection, we numerically solve a related model where we impose current biases in both horizontal and vertical directions such that $I_v = I_T = -I_B$ and $I_h = I_R = -I_L$ [see Fig. 1(b)]. The four superconducting phase variables adjust accordingly. The numerical calculations are based on evaluating convergence of the steepest descent algorithm for a multiterminal Josephson junction. A dichotomic search was implemented in order to locate the CCCs to high accuracy. We use $I_{k,l}^c \equiv I_P^c$ and $I_{k,l,(m)}^c \equiv I_q^c$ for the critical currents of the processes coupling to two and three superconducting phase variables, respectively. Figure 3 shows the CCCs of a four-terminal device with the transmission coefficient scaling factors $\tau_B = \tau_L = \tau_R = 1$ and different values of τ_T. For positive values of I_q^c/I_P^c, the CCCs have the shape of nested rounded rectangles. For sufficiently negative I_q^c/I_P^c however, the CCCs evolve from diamondlike to a shape presenting nonconvex sharp-angled points when lowering τ_T. Notably, the CCCs with nonconvex sharp-angled points are only obtained for a sufficiently negative Cooper quartet critical current (here $I_q^c/I_P^c = -0.2$), which is in agreement with the preceding analytical solution.

In Fig. 4(a) we further implement two weak links with $\tau_T,\ \tau_L \leqslant 1$, whereas, maintaining $\tau_B = \tau_R = 1$, and we use a negative Cooper quartet critical current $I_q^c/I_P^c = -0.2$. Focusing on the panels on the diagonal, i.e., $\tau_T = \tau_L = 1/4,\ 1/2,\ 1$, we obtain an evolution from diamondike to squarelike CCCs as $\tau_T = \tau_L$ decreases. Since a rectangular CCC is indicative of independent currents in orthogonal directions, this evolution demonstrates a loss of quantum mechanical coupling between I_v and I_h as the contact transmission coefficient scaling factor decreases. The intermediate value $\tau_T = \tau_L = 1/2$ yields reentrance on both supercurrent axes, which originate from the underlying diagonal mirror symmetry in the device. Considering now the off-diagonal panels in Fig. 4(a), we obtain shapes with nonconvex sharp-angled points on the I_v^c axis if $\tau_T = 1/4,\ 1/2$, and $\tau_L = 1$, and the same on the I_h^c axis if $\tau_T = 1$ and $\tau_L = 1/4,\ 1/2$. This is again in qualitative agreement with the analytical model calculations presented in the above Sec. IV A.

In Fig. 4(b), we introduce all possible higher-order two-terminal $I_{2T}'^c \sin[2(\varphi_i - \varphi_j)]$ coupling terms in addition to the Cooper quartets. We observe the robustness of the reentrant sharp-angled points with respect to addition of these. Qualitatively, this can be interpreted as due to the fact that a smooth feature on top of a sharp cusp does not alter the latter. Figures 4(c) and 4(d) comparatively show the CCCs with vanishingly small quartet critical current but with finite $I_{2T}'^c$ taking negative or positive values. The nonconvex sharp-angled points are absent in the corresponding CCCs if $I_q^c = 0$ and $I_{2T}'^c \neq 0$. Those nonconvex sharp-angled points are, thus, a unique signature of the nonlocally π-shifted Cooper quartets.

Eventually, we demonstrate robustness of the reentrant pockets upon including the DC-Josephson effect depending on all four superconducting phase variables [30]. At the lowest order in tunneling, the corresponding Josephson critical currents are denoted by $I_q'^c$, and they scale, such as $\tau_L\tau_R\tau_B\tau_T$. Figure 5 provides the CCCs for variable combinations of I_q^c/I_P^c and $I_q'^c/I_P^c$, and with $\tau_T \lesssim 1$ and $\tau_B = \tau_L = \tau_R = 1$. The data with $I_q^c \gtrsim 0$ reveal smooth nonreentrant variations, contrasting with the sharper reentrantlike variations on the other panels. We conclude that reentrant features in CCCs at negative Cooper quartet critical current I_q^c are robust with respect to including higher-order Josephson terms.

V. CONCLUSIONS

To conclude, it follows from basic theoretical arguments that the quartet supercurrent contribution must be π shifted with respect to the lowest-order Josephson Cooper

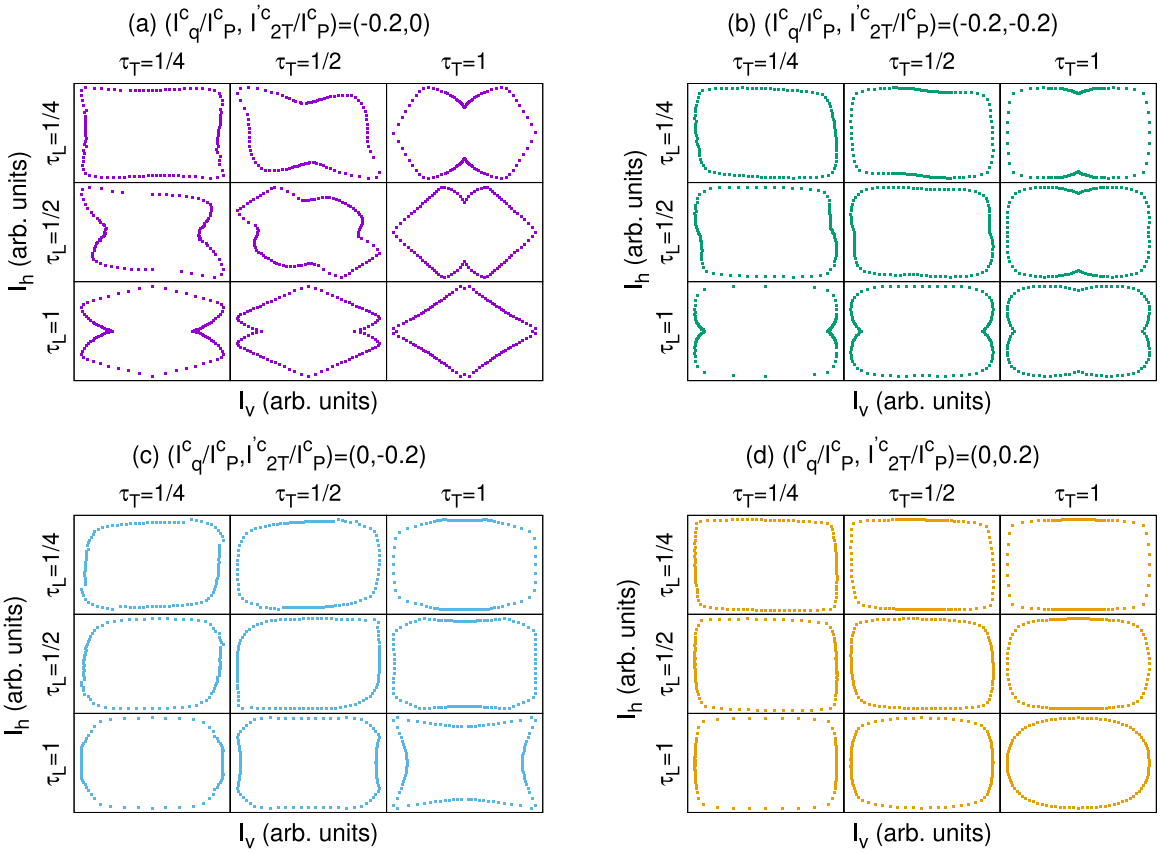

FIG. 4. Critical current contours in the (I_v, I_h) plane with $\tau_B = \tau_R = 1$ and with two weak links. The values $(I^c_q/I^c_P, I'^c_{2T}/I^c_P) = (-0.2, 0)$, $(-0.2, -0.2)$, $(0, -0.2)$, and (0,0.2) are used in panels [(a)–(d)], respectively. The panels are organized as a table, and the values of τ_L, τ_T are indicated. Each panel is rescaled to full size on the I_v and I_h axes. Polarization is with two orthogonal current biases, see Fig. 1(b). Temperature is set to zero.

pair supercurrent. We demonstrated that the nonconvex two-dimensional CCCs of a current-biased four-terminal Josephson junction are generically due to a relative π shift of the higher-order terms in the current-phase relation. These can either originate simply from the two-terminal Josephson current-phase relation or more interestingly from the Cooper quartets. Finally, we demonstrated that nonconvex sharp-angled points in the CCCs are a distinctive signature of negative Cooper critical current contributions. However, we note that too small negative quartet critical currents will restore convex CCC, which sets constraints on the transmissions for the observation of the characteristic reentrance. A recent experiment [38] reported the appearance of nonconvex CCCs only under applied magnetic field. However, in contrast to our assumptions, all contacts had large transparencies. Conclusive evidence for the π-shifted quartet term could be realized with bilayer graphene- or semiconducting-quantum point contacts [36,80] with tunable contact transparencies.

ACKNOWLEDGMENTS

We benefited from fruitful discussions with M. d'Astuto, S. Collienne, T. Klein, F. Lévy-Bertrand, M. A. Méasson, P. Rodière, and A. Silhanek. R.M. acknowledges a useful correspondence with V. E. Manucharyan. R.M. thanks the Infrastructure de Calcul Intensif et de Données (GRICAD) for use of the resources of the Mésocentre de Calcul Intensif de l'Université Grenoble-Alpes (CIMENT). This work was supported by the International Research Project SUPRADEVMAT between CNRS in Grenoble and KIT in Karlsruhe. This work received support from the French National Research Agency (ANR) in the framework of the Graphmon (Grant No. ANR-19-CE47-0007) and JOSPEC (Grant No. ANR-17-CE30-0030) projects. This work was partly supported by Helmholtz Society through Program STN and the DFG via the Project No. DA 1280/7-1.

APPENDIX A: DETAILS ON PHENOMENOLOGICALLY SQUARING THE SINGLE COOPER PAIR WAVE FUNCTION

In this Appendix, we detail how to deduce Eq. (2) from Eq. (1). Namely, we square the wave function of a Cooper pair split between S_i and S_j,

$$\psi^2 = \left[\frac{1}{\sqrt{2}}(c^+_{i,\uparrow}c^+_{j,\downarrow} - c^+_{i,\downarrow}c^+_{j,\uparrow})\right]^2 \tag{A1}$$

$$= \frac{1}{2}(c^+_{i,\uparrow}c^+_{j,\downarrow} - c^+_{i,\downarrow}c^+_{j,\uparrow})(c^+_{i,\uparrow}c^+_{j,\downarrow} - c^+_{i,\downarrow}c^+_{j,\uparrow}) \tag{A2}$$

$$= \frac{1}{2}[c^+_{i,\uparrow}c^+_{j,\downarrow}c^+_{i,\uparrow}c^+_{j,\downarrow} - c^+_{i,\uparrow}c^+_{j,\downarrow}c^+_{i,\downarrow}c^+_{j,\uparrow} - c^+_{i,\downarrow}c^+_{j,\uparrow}c^+_{i,\uparrow}c^+_{j,\downarrow} + c^+_{i,\downarrow}c^+_{j,\uparrow}c^+_{i,\downarrow}c^+_{j,\uparrow}] \tag{A3}$$

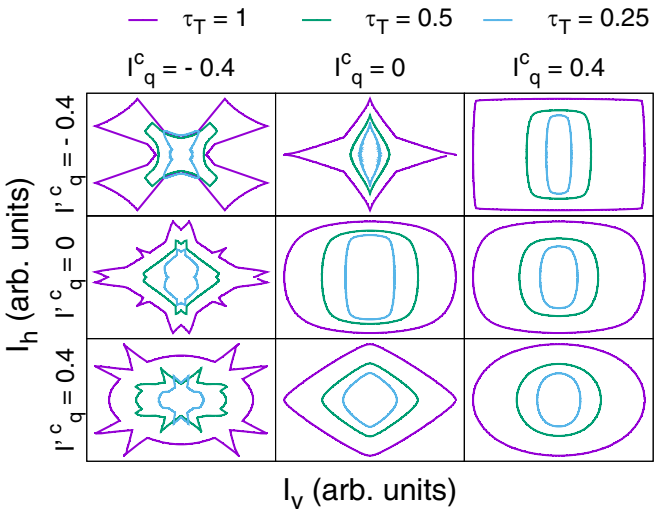

FIG. 5. Critical current contours on the (I_v, I_h) plane, in the presence of Josephson coupling to the four superconducting phase variables and with a single weak link. The contact transmission coefficients are such that $\tau_B = \tau_L = \tau_R = 1$ and $\tau_T = 1$ (magenta), $\tau_T = 0.5$ (green) and $\tau_T = 0.25$ (blue). The different panels are organized, such as a table, and the values of I_q^c and $I_q^{\prime c}$ are indicated on the figure, both of those being normalized to $I_P^c = 1$. Each panel is rescaled to full size on the I_v and I_h axes. Polarization is with two orthogonal current biases, see Fig. 1(b). Temperature is set to zero.

$$= \frac{1}{2}[-(c^+_{i,\uparrow})^2(c^+_{j,\downarrow})^2 - (c^+_{i,\uparrow}c^+_{i,\downarrow})(c^+_{j,\uparrow}c^+_{j,\downarrow}) - (c^+_{i,\uparrow}c^+_{i,\downarrow})(c^+_{j,\uparrow}c^+_{j,\downarrow}) - (c^+_{i,\downarrow})^2(c^+_{j,\uparrow})^2]. \quad \text{(A4)}$$

Evaluating quantum-mechanical expectation values in the final state leads to

$$\langle\psi^2\rangle = -\langle c^+_{i,\uparrow}c^+_{i,\downarrow}\rangle\langle c^+_{j,\uparrow}c^+_{j,\downarrow}\rangle, \quad \text{(A5)}$$

where we used $\langle(c^+_{i,\uparrow})^2\rangle = 0$ because of spin conservation. The above Eq. (A5) matches the above Eq. (2).

APPENDIX B: DETAILS ON A SINGLE SUPERCONDUCTING WEAK LINK

In this Appendix, we evaluate the first- and second-order harmonics of the Josephson current-phase relation for a single-channel superconducting weak link having hopping amplitude J_0, and connecting the left and right superconducting leads S_L and S_R with superconducting phases φ_L and φ_R, respectively. The Andreev bound state (ABS) energies take the following form:

$$E_\pm(\varphi_R - \varphi_L, \alpha) = \pm\Delta\sqrt{1 - \alpha\,\sin^2\left(\frac{\varphi_R - \varphi_L}{2}\right)}, \quad \text{(B1)}$$

where the dimensionless normal-state transmission coefficient α between 0 and 1 is given by

$$\alpha = \frac{4(J_0/W)^2}{[1 + (J_0/W)^2]^2}. \quad \text{(B2)}$$

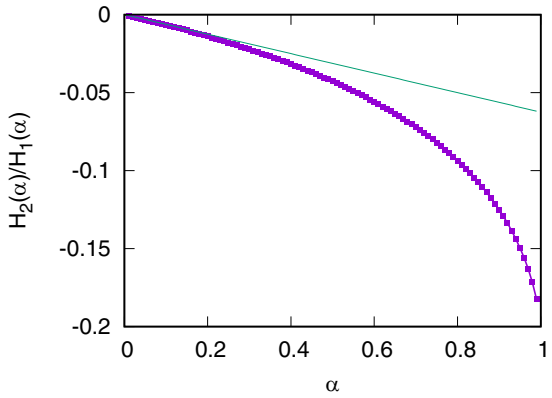

FIG. 6. The figure shows $H_2(\alpha)/H_1(\alpha)$ as a function of the normal-state contact transparency α (magenta datapoints), where $H_1(\alpha)$ and $H_2(\alpha)$ are the first and second harmonics of the Josephson energy, see Eqs. (B8) and (B9). The green line shows a comparison to $H_2(\alpha)/H_1(\alpha) = -\alpha/16$, see Eq. (B7).

The ABS energies are expressed as

$$E_\pm(\varphi_R - \varphi_L, \alpha) = \pm\Delta\sqrt{1 - \frac{\alpha}{2} + \frac{\alpha}{2}\cos(\varphi_R - \varphi_L)} \quad \text{(B3)}$$

$$= \pm\Delta\sqrt{1 - \frac{\alpha}{2}}\sqrt{1 + \frac{\alpha}{2-\alpha}\cos(\varphi_R - \varphi_L)}. \quad \text{(B4)}$$

Expanding to second order, we obtain

$$E_\pm(\varphi_R - \varphi_L, \alpha) = \pm\Delta\sqrt{1 - \frac{\alpha}{2}}\left\{1 + \frac{\alpha}{2(2-\alpha)}\cos(\varphi_R - \varphi_L) - \frac{1}{8}\left(\frac{\alpha}{2-\alpha}\right)^2\cos^2(\varphi_R - \varphi_L)\right\} + \cdots \quad \text{(B5)}$$

Using $\cos^2(\varphi_R - \varphi_L) = \{1 + \cos[2(\varphi_R - \varphi_L)]\}/2$, we obtain

$$E_\pm(\varphi_R - \varphi_L, \alpha) = \pm[E_0^J + E_{2e}^J\cos(\varphi_R - \varphi_L) + E_{4e}^J\cos[(\varphi_R - \varphi_L)] + \cdots], \quad \text{(B6)}$$

with

$$\frac{E_{4e}^J}{E_{2e}^J} = -\frac{\alpha}{16}, \quad \text{(B7)}$$

in the small-α limit, where $E_{2e}^J > 0$ is positive and $E_{4e}^J < 0$ is negative.

Now, we present supplemental numerical calculations for the amplitudes $H_1(\alpha)$ and $H_2(\alpha)$ of the first and second Josephson harmonics as a function of the dimensionless normal-state transmission coefficient α,

$$H_1(\alpha) = \int_0^{2\pi}\frac{d\varphi}{2\pi}E_+(\varphi, \alpha)\cos\,\varphi, \quad \text{(B8)}$$

$$H_2(\alpha) = \int_0^{2\pi}\frac{d\varphi}{2\pi}E_+(\varphi, \alpha)\cos(2\varphi). \quad \text{(B9)}$$

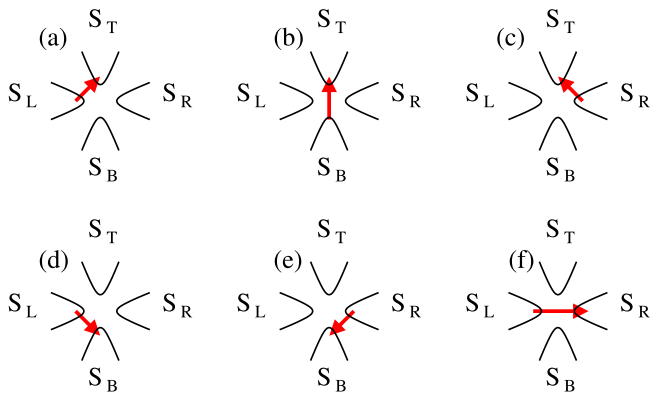

FIG. 7. The figure shows the six two-terminal processes transferring Cooper pairs between the superconducting leads.

Figure 6 shows that $H_2(\alpha)/H_1(\alpha) < 0$ is negative for all values of $\alpha < 1$. The limiting behavior $H_2(\alpha)/H_1(\alpha) = -\alpha/16$ is obtained at small α, in agreement with the above Eq. (B7).

APPENDIX C: DETAILS ON THE DEVICE CONTROLLED WITH ONE CURRENT AND ONE PHASE BIAS

In this Appendix, we consider the multiterminal Josephson circuit shown in the above Fig. 1(a), consisting of the four superconducting leads S_L, S_R, S_B, and S_T with the phases φ_L, φ_R, φ_B, and φ_T. The phase difference $\varphi_R - \varphi_L = \Phi$ is controlled by the flux Φ in the loop, and supercurrent $I_v = I_B = -I_T$ is forced to flow from the bottom to the top superconducting leads. We use the notation $\varphi_T = \psi$. Given those constraints, the supercurrent transmitted into S_T is parametrized by a single phase variable, for instance, by the phase variable ψ, and the critical current from bottom to top is obtained by maximizing the supercurrent $I_v(\psi)$ over ψ.

The superconductor S_T is assumed to be connected to the normal conductor N_0 by hopping amplitude that is weaker than the others. A reduction factor τ_T is applied to each Cooper pair crossing the $N_0 - S_T$ interface.

First considering vanishing small quartet Josephson energy $I_q^c = 0$, we obtain the following expression of the four-terminal Josephson junction energy $E^{(0)}$:

$$\begin{aligned} E^{(0)} = {} & E_P\tau_T\{\cos(\varphi_T - \varphi_L) + \cos(\varphi_T - \varphi_B) \\ & + \cos(\varphi_T - \varphi_R)\} \\ & + E_P\{\cos(\varphi_B - \varphi_L) + \cos(\varphi_B - \varphi_R) \\ & + \cos(\varphi_R - \varphi_L)\}, \end{aligned} \tag{C1}$$

where E_P is the Josephson energy associated to transferring Cooper pairs between the leads. Each term entering Eq. (C1) is schematically shown in Fig. 7. Using $\varphi_L = -\varphi_R = -\varphi/2$ and $\varphi_T = \psi$, we obtain

$$\begin{aligned} E^{(0)} = {} & E_P\tau_T\left\{\cos\left(\psi + \frac{\varphi}{2}\right) + \cos\left(\psi - \varphi_B\right) + \cos\left(\psi - \frac{\varphi}{2}\right)\right\} \\ & + E_P\left\{\cos\left(\varphi_B + \frac{\varphi}{2}\right) + \cos\left(\varphi_B - \frac{\varphi}{2}\right) + \cos\,\varphi\right\}. \end{aligned} \tag{C2}$$

Then,

$$I_T = -\frac{2e}{\hbar}\frac{\partial E^{(0)}}{\partial \psi} \tag{C3}$$

$$\begin{aligned} = {} & \frac{2eE_P\tau_T}{\hbar}\left\{\sin\left(\psi + \frac{\varphi}{2}\right) + \sin(\psi - \varphi_B)\right. \\ & \left. + \sin\left(\psi - \frac{\varphi}{2}\right)\right\} \end{aligned} \tag{C4}$$

$$I_B = -\frac{2e}{\hbar}\frac{\partial E^{(0)}}{\partial \varphi_B} \tag{C5}$$

$$\begin{aligned} = {} & \frac{2eE_P\tau_T}{\hbar}\sin(\varphi_B - \psi) \\ & + \frac{2E_P}{\hbar}\left\{\sin\left(\varphi_B + \frac{\varphi}{2}\right) + \sin\left(\varphi_B - \frac{\varphi}{2}\right)\right\}. \end{aligned} \tag{C6}$$

The current source imposes

$$I_T + I_B = -(2e/\hbar)[\partial E^{(0)}/\partial\psi + \partial E^{(0)}/\partial\varphi_B] = 0, \tag{C7}$$

which leads to the self-consistent $\varphi_B = \varphi_B^*$ with

$$\sin\,\varphi_B^* = -\tau_T \sin\,\psi, \tag{C8}$$

showing that φ_B^* is on the order of τ_T. Then, at the order of τ_T, we obtain

$$I_T = -\frac{2e}{\hbar}\frac{\partial E^{(0)}}{\partial\psi} \simeq \frac{2eE_P\tau_T}{\hbar}\left[1 + 2\cos\left(\frac{\varphi}{2}\right)\right]\sin\,\psi. \tag{C9}$$

Taking the maximum over ψ and expanding in small φ leads to following expansion of the critical current flowing from bottom to top at small φ, at the order of τ_T:

$$I_c \simeq \frac{2eE_P\tau_T}{\hbar}\left[3 - \frac{\varphi^2}{4}\right], \tag{C10}$$

leading to convex CCC in the absence of the quartets. Equation (C10) is rewritten as

$$I_c \simeq \tau_T I_P^c\left[3 - \frac{\varphi^2}{4}\right], \tag{C11}$$

where $I_P^c = 2eE_P/\hbar$ is related to the Cooper pair critical current.

Now, we include finite but small quartet Josephson energy E_q. Those processes are shown in Fig. 8, and, at the order of τ_T, they yield the following correction $\delta E^{(0)}$ to the energy $E^{(0)}$ in Eq. (C1):

$$\begin{aligned} \delta E^{(0)} = {} & E_q\{\tau_T\cos(\varphi_L + \varphi_T - 2\varphi_B) + \tau_T\cos(\varphi_R + \varphi_T - 2\varphi_B) \\ & + \cos(\varphi_R + \varphi_L - 2\varphi_B) + \tau_T\cos(\varphi_T + \varphi_R - 2\varphi_L) \\ & + \tau_T\cos(\varphi_T + \varphi_B - 2\varphi_L) + \cos(\varphi_R + \varphi_B - 2\varphi_L) \\ & + \tau_T\cos(\varphi_T + \varphi_L - 2\varphi_R) + \tau_T\cos(\varphi_T + \varphi_B - 2\varphi_R) \\ & + \cos(\varphi_L + \varphi_B - 2\varphi_R)\}. \end{aligned} \tag{C12}$$

Then, we find

$$\begin{aligned} -\frac{\partial\delta E^{(0)}}{\partial\varphi_T} = {} & \tau_T E_q\{\sin(\varphi_L + \varphi_T - 2\varphi_B) \\ & + \sin(\varphi_R + \varphi_T - 2\varphi_B) + \sin(\varphi_T + \varphi_R - 2\varphi_L) \end{aligned}$$

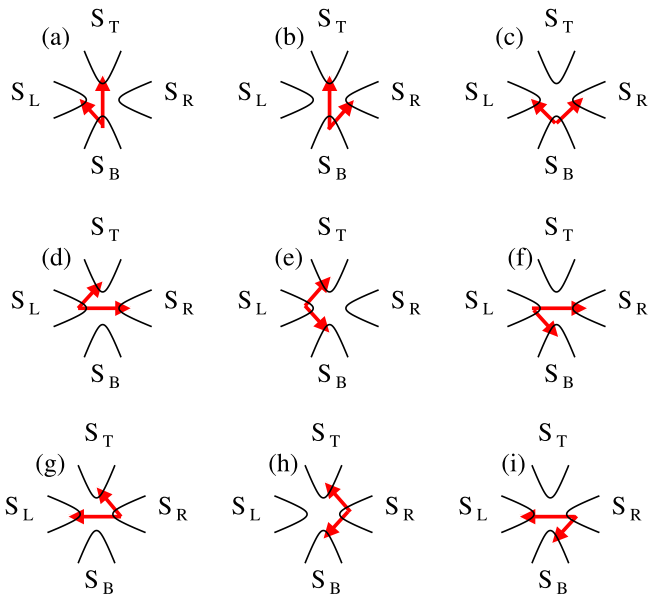

FIG. 8. The figure shows the nine three-terminal processes transferring Cooper quartets between the superconducting leads, at the orders $(\tau_T)^0$ and τ_T. The three higher-order processes of order $(\tau_T)^2$ are not shown in the figure.

$$+\sin(\varphi_T+\varphi_B-2\varphi_L)+\sin(\varphi_T+\varphi_L-2\varphi_R)$$
$$+\sin(\varphi_T+\varphi_B-2\varphi_R)\} \tag{C13}$$
$$=\tau_T E_q\Big\{\sin\Big(-\frac{\varphi}{2}+\psi-2\varphi_B\Big)+\sin\Big(\frac{\varphi}{2}+\psi-2\varphi_B\Big)$$
$$+\sin\Big(\psi+\frac{3\varphi}{2}\Big)+\sin(\psi+\varphi_B+\varphi)$$
$$+\sin\Big(\psi-\frac{3\varphi}{2}\Big)+\sin(\psi+\varphi_B-\varphi)\Big\}. \tag{C14}$$

Since φ_B is on the order of τ_T [see the above Eq. (C8)], we replace φ_B by $\varphi_B=0$ in the above Eqs. (C13) and (C14) to obtain the order-τ_T contribution to $-\partial\delta E^{(0)}/\partial\varphi_T$,

$$-\frac{\partial\delta E^{(0)}}{\partial\varphi_T}\simeq\tau_T E_q\Big\{\sin\Big(-\frac{\varphi}{2}+\psi\Big)+\sin\Big(\frac{\varphi}{2}+\psi\Big)$$
$$+\sin\Big(\psi+\frac{3\varphi}{2}\Big)+\sin(\psi+\varphi)$$
$$+\sin\Big(\psi-\frac{3\varphi}{2}\Big)+\sin(\psi-\varphi)\Big\} \tag{C15}$$
$$=2\tau_T E_q\Big\{\cos\Big(\frac{\varphi}{2}\Big)+\cos\varphi+\cos\Big(\frac{3\varphi}{2}\Big)\Big\}\sin\psi. \tag{C16}$$

Considering now $-\partial\delta E^{(0)}/\partial\varphi_B$, we find

$$-\frac{\partial\delta E^{(0)}}{\partial\varphi_B}=E_q\{2\tau_T\sin(2\varphi_B-\varphi_L-\varphi_T)$$
$$+2\tau_T\sin(2\varphi_B-\varphi_R-\varphi_T)$$
$$+2\sin(2\varphi_B-\varphi_R-\varphi_L)$$
$$+\tau_T\sin(\varphi_T+\varphi_B-2\varphi_L)$$
$$+\sin(\varphi_R+\varphi_B-2\varphi_L)$$
$$+\tau_T\sin(\varphi_T+\varphi_B-2\varphi_R)$$
$$+\sin(\varphi_L+\varphi_B-2\varphi_R)\} \tag{C17}$$
$$=E_q\Big\{2\tau_T\sin\Big(2\varphi_B+\frac{\varphi}{2}-\psi\Big)$$
$$+2\tau_T\sin\Big(2\varphi_B-\frac{\varphi}{2}-\psi\Big)$$
$$+2\sin(2\varphi_B)+\tau_T\sin(\psi+\varphi_B+\varphi)$$
$$+\sin\Big(\varphi_B+\frac{3\varphi}{2}\Big)+\tau_T\sin(\psi+\varphi_B-\varphi)$$
$$+\sin\Big(\varphi_B-\frac{3\varphi}{2}\Big)\Big\}. \tag{C18}$$

The phase variable φ_B turns out to be linear in τ_T at $E_q=0$ [see the above Eq. (C8)]. At small E_q, both $-\partial\delta E^{(0)}/\partial\varphi_T$ and $-\partial\delta E^{(0)}/\partial\varphi_B$ are on the order of $E_q\tau_T$. Then, φ_B^* is linear in τ_T in the presence of small E_q as was the case for $E_q=0$.

The supercurrent transmitted into the superconducting lead S_T is then given by the sum of Eqs. (C9) and (C16),

$$I_T=-\frac{2e}{\hbar}\frac{\partial(E^{(0)}+\delta E^{(0)})}{\partial\psi} \tag{C19}$$
$$\simeq\frac{2e\tau_T E_P}{\hbar}\Big\{3+6\frac{E_q}{E_P}-\frac{\varphi^2}{4}\Big[1+14\frac{E_q}{E_P}\Big]\Big\}\sin\psi. \tag{C20}$$

Taking the maximum over ψ leads to the following expression of the critical current:

$$I_v^c=-\frac{2e}{\hbar}\frac{\partial(E^{(0)}+\delta E^{(0)})}{\partial\psi} \tag{C21}$$
$$\simeq\frac{2e\tau_T E_P}{\hbar}\Big\{3+6\frac{E_q}{E_P}-\frac{\varphi^2}{4}\Big[1+14\frac{E_q}{E_P}\Big]\Big\}. \tag{C22}$$

Equation (C21) is rewritten as

$$I_v^c=\tau_T I_P^c\Big\{3+6\frac{I_q^c}{I_P^c}-\frac{\varphi^2}{4}\Big[1+14\frac{I_q^c}{I_P^c}\Big]\Big\}, \tag{C23}$$

where $I_P^c=2eE_P/\hbar$ and $I_q^c=2eE_q/\hbar$ are related to the Cooper pair and Cooper quartet critical currents. This concludes the demonstration of the above Eq. (6). Equation (C23) goes to Eq. (C11) in the $I_q^c\to 0$ limit of vanishingly small quartet energy. As a consequence of Eq. (C23), the CCC is nonconvex if

$$I_q^c<-\frac{I_P^c}{14}, \tag{C24}$$

thus, necessarily being negative.

[1] F. Arute *et al.*, Quantum supremacy using a programmable superconducting processor, Nature (London) **574**, 505 (2019).

[2] J. M. Byers and M. E. Flatté, Probing Spatial Correlations with Nanoscale Two-Contact Tunneling, Phys. Rev. Lett. **74**, 306 (1995).

[3] J. Torrès and T. Martin, Positive and negative Hanbury-Brown and Twiss correlations in normal metal-superconducting devices, Eur. Phys. J. B **12**, 319 (1999).

[4] G. Deutscher and D. Feinberg, Coupling superconducting-ferromagnetic point contacts by Andreev reflections, Appl. Phys. Lett. **76**, 487 (2000).

[5] M. S. Choi, C. Bruder, and D. Loss, Spin-dependent Josephson current through double quantum dots and measurement of entangled electron states, Phys. Rev. B **62**, 13569 (2000).

[6] P. Samuelsson and M. Büttiker, Chaotic Dot-Superconductor Analog of the Hanbury Brown–Twiss effect, Phys. Rev. Lett. **89**, 046601 (2002).

[7] N. M. Chtchelkatchev, G. Blatter, G. B. Lesovik, and T. Martin, Bell inequalities and entanglement in solid-state devices, Phys. Rev. B **66**, 161320(R) (2002).

[8] R. Mélin and D. Feinberg, Sign of the crossed conductances at a ferromagnet/superconductor/ferromagnet double interface, Phys. Rev. B **70**, 174509 (2004).

[9] A. L. Yeyati, F. S. Bergeret, A. Martín-Rodero, and T. M. Klapwijk, Entangled Andreev pairs and collective excitations in nanoscale superconductors, Nat. Phys. **3**, 455 (2007).

[10] R. Mélin, C. Benjamin, and T. Martin, Positive cross correlations of noise in superconducting hybrid structures: Roles of interfaces and interactions, Phys. Rev. B **77**, 094512 (2008).

[11] A. Freyn, M. Flöser, and R. Mélin, Positive current cross-correlations in a highly transparent normal-superconducting beam splitter due to synchronized Andreev and inverse Andreev reflections, Phys. Rev. B **82**, 014510 (2010).

[12] M. Flöser, D. Feinberg, and R. Mélin, Absence of split pairs in cross correlations of a highly transparent normal metal–superconductor–normal metal electron-beam splitter, Phys. Rev. B **88**, 094517 (2013).

[13] D. Beckmann, H. B. Weber, and H. V. Löhneysen, Evidence for Crossed Andreev Reflection in Superconductor-Ferromagnet Hybrid Structures, Phys. Rev. Lett. **93**, 197003 (2004).

[14] S. Russo, M. Kroug, T. M. Klapwijk, and A. F. Morpurgo, Experimental Observation of Bias-Dependent Nonlocal Andreev Reflection, Phys. Rev. Lett. **95**, 027002 (2005).

[15] P. Cadden-Zimansky and V. Chandrasekhar, Nonlocal Correlations in Normal-Metal Superconducting Systems, Phys. Rev. Lett. **97**, 237003 (2006).

[16] L. Hofstetter, S. Csonka, J. Nygard, and C. Schönenberger, Cooper pair splitter realized in a two-quantum-dot Y-junction, Nature (London) **461**, 960 (2009).

[17] L. G. Herrmann, F. Portier, P. Roche, A. Levy Yeyati, T. Kontos, and C. Strunk, Carbon Nanotubes as Cooper-Pair Beam Splitters, Phys. Rev. Lett. **104**, 026801 (2010).

[18] Z. B. Tan, D. Cox, T. Nieminen, P. Lähteenmäki, D. Golubev, G. B. Lesovik, and P. J. Hakonen, Cooper Pair Splitting by Means of Graphene Quantum Dots, Phys. Rev. Lett. **114**, 096602 (2015).

[19] I. V. Borzenets, Y. Shimazaki, G. F. Jones, M. F. Craciun, S. Russo, M. Yamamoto, and S. Tarucha, High efficiency CVD graphene-lead (Pb) Cooper pair splitter, Sci. Rep. **6**, 23051 (2016).

[20] P. Pandey, R. Danneau, and D. Beckmann, Ballistic Graphene Cooper Pair Splitter, Phys. Rev. Lett. **126**, 147701 (2021).

[21] A. Das, Y. Ronen, M. Heiblum, D. Mahalu, A. V. Kretinin, and H. Shtrikman, High-efficiency Cooper pair splitting demonstrated by two-particle conductance resonance and positive noise cross- correlation, Nat. Commun. **3**, 1165 (2012).

[22] R. de Bruyn Ouboter and A. Omelyanchouk, Multi-terminal squid controlled by the transport current, Physica B **205**, 153 (1995).

[23] M. Amin, A. Omelyanchouk, and A. Zagoskin, Mesoscopic multiterminal Josephson structures. I. Effects of nonlocal weak coupling, Low Temp. Phys. **27**, 616 (2001).

[24] M. Amin, A. Omelyanchouk, and A. Zagoskin, DC SQUID based on the mesoscopic multiterminal Josephson junction, Physica C **372-376**, 178 (2002).

[25] M. Amin, A. Omelyanchouk, A. Blais, A. M. van den Brink, G. Rose, T. Duty, and A. Zagoskin, Multi-terminal superconducting phase qubit, Physica C **368**, 310 (2002).

[26] J. C. Cuevas and H. Pothier, Voltage-induced Shapiro steps in a superconducting multiterminal structure, Phys. Rev. B **75**, 174513 (2007).

[27] A. Freyn, B. Douçot, D. Feinberg, and R. Mélin, Production of Nonlocal Quartets and Phase-Sensitive Entanglement in a Superconducting Beam Splitter, Phys. Rev. Lett. **106**, 257005 (2011).

[28] T. Jonckheere, J. Rech, T. Martin, B. Douçot, D. Feinberg, and R. Mélin, Multipair DC Josephson resonances in a biased allsuperconducting bijunction, Phys. Rev. B **87**, 214501 (2013).

[29] R. Mélin, D. Feinberg, and B. Douçot, Partially resummed perturbation theory for multiple Andreev reflections in a short three-terminal Josephson junction, Eur. Phys. J. B **89**, 67 (2016).

[30] R. Mélin, Inversion in a four terminal superconducting device on the quartet line. I. Two-dimensional metal and the quartet beam splitter, Phys. Rev. B **102**, 245435 (2020).

[31] A. Melo, V. Fatemi, and A. R. Akhmerov, Multiplet supercurrent in Josephson tunneling circuits, SciPost Phys. **12**, 017 (2022).

[32] R. Mélin and D. Feinberg, Quantum interferometer for quartets in superconducting three-terminal Josephson junctions, Phys. Rev. B **107**, L161405 (2023).

[33] A. H. Pfeffer, J. E. Duvauchelle, H. Courtois, R. Mélin, D. Feinberg, and F. Lefloch, Subgap structure in the conductance of a three-terminal Josephson junction, Phys. Rev. B **90**, 075401 (2014).

[34] Y. Cohen, Y. Ronen, J. H. Kang, M. Heiblum, D. Feinberg, R. Mélin, and H. Strikman, Non-local supercurrent of quartets in a three-terminal Josephson junction, Proc. Natl. Acad. Sci. USA **115**, 6991 (2018).

[35] K. F. Huang, Y. Ronen, R. Mélin, D. Feinberg, K. Watanabe, T. Taniguchi, and P. Kim, Evidence for 4*e* charge of Cooper quartets in a biased multi-terminal graphene-based Josephson junction, Nat. Commun. **13**, 3032 (2022).

[36] G. V. Graziano, M. Gupta, M. Pendharkar, J. T. Dong, C. P. Dempsey, C. Palmstrøm, and V. S. Pribiag, Selective control of conductance modes in multi-terminal Josephson junctions, Nat. Commun. **13**, 5933 (2022).

[37] A. W. Draelos, M.-T. Wei, A. Seredinski, H. Li, Y. Mehta, K. Watanabe, T. Taniguchi, I. V. Borzenets, F. Amet, and

G. Finkelstein, Supercurrent flow in multiterminal graphene Josephson junctions, Nano Lett. **19**, 1039 (2019).

[38] N. Pankratova, H. Lee, R. Kuzmin, K. Wickramasinghe, W. Mayer, J. Yuan, M. Vavilov, J. Shabani, and V. Manucharyan, Multiterminal Josephson Effect, Phys. Rev. X **10**, 031051 (2020).

[39] G. V. Graziano, J. S. Lee, M. Pendharkar, C. Palmstrøm, and V. S. Pribiag, Transport studies in a gate-tunable three-terminal Josephson junction, Phys. Rev. B **101**, 054510 (2020).

[40] E. G. Arnault, T. Larson, A. Seredinski, L. Zhao, H. Li, K. Watanabe, T. Taniguchi, I. Borzenets, F. Amet, and G. Finkelstein, The multiterminal inverse AC Josephson effect, Nano Lett. **21**, 9668 (2021).

[41] S. A. Khan, L. Stampfer, T. Mutas, J.-H. Kang, P. Krogstrup, and T. S. Jespersen, Multiterminal quantized conductance in InSb nanocrosses, Adv. Mater. **33**, 2100078 (2021).

[42] E. G. Arnault, S. Idris, A. McConnell, L. Zhao, T. F. Q. Larson, K. Watanabe, T. Taniguchi, G. Finkelstein, and F. Amet, Dynamical stabilization of multiplet supercurrents in multiterminal Josephson junctions, Nano Lett. **22**, 7073 (2022).

[43] S. Matsuo, J. S. Lee, C.-Y. Chang, Y. Sato, K. Ueda, C. J. Palstrøm, and S. Tarucha, Observation of the nonlocal Josephson effect on double InAs nanowires, Commun. Phys. **5**, 221 (2022).

[44] F. Zhang, A. S. Rashid, M. T. Ahari, W. Zhang, K. M. Ananthanarayanan, R. Xiao, G. J. de Coster, M. J. Gilbert, N. Samarth, and M. Kayyalha, Andreev processes in mesoscopic multi-terminal graphene Josephson junctions, Phys. Rev. B **107**, L140503 (2023).

[45] R. Mélin, J.-G. Caputo, K. Yang, and B. Douçot, Simple Floquet-Wannier-Stark-Andreev viewpoint and emergence of low-energy scales in a voltage-biased three-terminal Josephson junction, Phys. Rev. B **95**, 085415 (2017).

[46] R. Mélin, R. Danneau, K. Yang, J.-G. Caputo, and B. Douçot, Engineering the Floquet spectrum of superconducting multiterminal quantum dots, Phys. Rev. B **100**, 035450 (2019).

[47] B. Douçot, R. Danneau, K. Yang, J.-G. Caputo, and R. Mélin, Berry phase in superconducting multiterminal quantum dots, Phys. Rev. B **101**, 035411 (2020).

[48] R. Mélin and B. Douçot, Inversion in a four terminal superconducting device on the quartet line. II. Quantum dot and Floquet theory, Phys. Rev. B **102**, 245436 (2020).

[49] R. Mélin, Ultralong-distance quantum correlations in three-terminal Josephson junctions, Phys. Rev. B **104**, 075402 (2021).

[50] S. Park, W. Lee, S. Jang, Y.-B. Choi, J. Park, W. Jung, K. Watanabe, T. Taniguchi, G. Y. Cho, and G.-H. Lee, Steady Floquet-Andreev states in graphene Josephson junctions, Nature (London) **603**, 421 (2022).

[51] R. Mélin, Multiterminal ballistic Josephson junctions coupled to normal leads, Phys. Rev. B **105**, 155418 (2022).

[52] A. Keliri and B. Douçot, Driven Andreev molecule, Phys. Rev. B **107**, 094505 (2023); Long-range coupling between superconducting dots induced by periodic driving, arXiv:2304.05987.

[53] J.-D. Pillet, V. Benzoni, J. Griesmar, J.-L. Smirr, and Ç.Ö. Girit, Nonlocal Josephson effect in Andreev molecules, Nano Lett. **19**, 7138 (2019).

[54] J.-D. Pillet, V. Benzoni, J. Griesmar, J.-L. Smirr, and Ç. Ö. Girit, Scattering description of Andreev molecules, SciPost Phys. Core **2**, 009 (2020).

[55] V. Kornich, H. S. Barakov, and Y. V. Nazarov, Fine energy splitting of overlapping Andreev bound states in multiterminal superconducting nanostructures, Phys. Rev. Res. **1**, 033004 (2019).

[56] O. Kürtössy, Z. Scherübl, G. Fülöp, I. E. Lukács, T. Kanne, J. Nygard, P. Makk, and S. Csonka, Andreev molecule in parallel InAs nanowires, Nano Lett. **21**, 7929 (2021).

[57] M. Coraiola, D. Z. Haxell, D. Sabonis, H. Weisbrich, A. E. Svetogorov, M. Hinderling, S. C. ten Kate, E. Cheah, F. Krizek, R. Schott, W. Wegscheider, J. C. Cuevas, W. Belzig, and F. Nichele, Hybridisation of Andreev bound states in three-terminal Josephson junctions, arXiv:2302.14535.

[58] S. Matsuo, T. Imoto, T. Yokoyama, Y. Sato, T. Lindemann, S. Gronin, G. C. Gardner, S. Nakosai, Y. Tanaka, M. J. Manfra, and S. Tarucha, Phase-dependent Andreev molecules and superconducting gap closing in coherently coupled Josephson junctions, arXiv:2303.10540.

[59] S. Matsuo, T. Imoto, T. Yokoyama, Y. Sato, T. Lindemann, S. Gronin, G. C. Gardner, M. J. Manfra, and S. Tarucha, Engineering of anomalous Josephson effect in coherently coupled Josephson junctions, arXiv:2305.06596.

[60] B. van Heck, S. Mi, and A. R. Akhmerov, Single fermion manipulation via superconducting phase differences in multiterminal Josephson junctions, Phys. Rev. B **90**, 155450 (2014).

[61] C. Padurariu, T. Jonckheere, J. Rech, R. Mélin, D. Feinberg, T. Martin, and Y. V. Nazarov, Closing the proximity gap in a metallic Josephson junction between three superconductors, Phys. Rev. B **92**, 205409 (2015).

[62] E. Strambini, S. D'Ambrosio, F. Vischi, F. S. Bergeret, Y. V. Nazarov, and F. Giazotto, The ω-SQUIPT as a tool to phase-engineer Josephson topological materials, Nat. Nanotechnol. **11**, 1055 (2016).

[63] R.-P. Riwar, M. Houzet, J. S. Meyer, and Y. V. Nazarov, Multi-terminal Josephson junctions as topological materials, Nat. Commun. **7**, 11167 (2016).

[64] E. Eriksson, R.-P. Riwar, M. Houzet, J. S. Meyer, and Y. V. Nazarov, Topological transconductance quantization in a four-terminal Josephson junction, Phys. Rev. B **95**, 075417 (2017).

[65] H.-Y. Xie, M. G. Vavilov, and A. Levchenko, Topological Andreev bands in three-terminal Josephson junctions, Phys. Rev. B **96**, 161406(R) (2017).

[66] H.-Y. Xie, M. G. Vavilov, and A. Levchenko, Weyl nodes in Andreev spectra of multiterminal Josephson junctions: Chern numbers, conductances and supercurrents, Phys. Rev. B **97**, 035443 (2018).

[67] O. Deb, K. Sengupta, and D. Sen, Josephson junctions of multiple superconducting wires, Phys. Rev. B **97**, 174518 (2018).

[68] B. Venitucci, D. Feinberg, R. Mélin, and B. Douçot, Nonadiabatic Josephson current pumping by microwave irradiation, Phys. Rev. B **97**, 195423 (2018).

[69] L. Peralta Gavensky, G. Usaj, D. Feinberg, and C. A. Balseiro, Berry curvature tomography and realization of topological Haldane model in driven three-terminal Josephson junctions, Phys. Rev. B **97**, 220505(R) (2018).

[70] R. L. Klees, G. Rastelli, J. C. Cuevas, and W. Belzig, Microwave Spectroscopy Reveals the Quantum Geometric Tensor of Topological Josephson Matter, Phys. Rev. Lett. **124**, 197002 (2020).

[71] V. Fatemi, A. R. Akhmerov, and L. Bretheau, Weyl Josepshon circuits, Phys. Rev. Res. **3**, 013288 (2021).

[72] L. Peyruchat, J. Griesmar, J.-D. Pillet, and Ç. Ö. Girit, Transconductance quantization in a topological Josephson tunnel junction circuit, Phys. Rev. Res. **3**, 013289 (2021).

[73] H. Weisbrich, R. L. Klees, G. Rastelli, and W. Belzig, Second chern number and non-abelian berry phase in topological superconducting systems, PRX Quantum **2**, 010310 (2021).

[74] Y. Chen and Y. V. Nazarov, Weyl point immersed in a continuous spectrum: An example from superconducting nanostructures, Phys. Rev. B **104**, 104506 (2021).

[75] Y. Chen and Y. V. Nazarov, Spin-Weyl quantum unit: Theoretical proposal, Phys. Rev. B **103**, 045410 (2021).

[76] E. V. Repin and Y. V. Nazarov, Weyl points in the multi-terminal hybrid superconductor-semiconductor nanowire devices, Phys. Rev. B **105**, L041405 (2022).

[77] L. Peralta Gavensky, G. Usaj, and C. A. Balseiro, Multiterminal Josephson junctions: A road to topological flux networks, Europhys. Lett. **141**, 36001 (2023).

[78] M. Gupta, G. V. Graziano, M. Pendharkar, J. T. Dong, C. P. Dempsey, C. Palmstrøm, and V. S. Pribiag, Superconducting diode effect in a three-terminal Josephson device, Nat. Commun. **14**, 3078 (2023).

[79] F. Zhang, M. T. Ahari, A. S. Rashid, G. J. de Coster, T. Taniguchi, K. Watanabe, M. J. Gilbert, N. Samarth, and M. Kayyalha, Reconfigurable magnetic-field-free superconducting diode effect in multi-terminal Josephson junctions, arXiv:2301.05081.

[80] R. Kraft, J. Mohrmann, R. Du, P. B. Selvasundaram, M. Irfan, U. N. Kanilmaz, F. Wu, D. Beckmann, H. von Löhneysen, R. Krupke, A. Akhmerov, I. Gornyi, and R. Danneau, Tailoring supercurrent confinement in graphene bilayer weak links, Nat. Commun. **9**, 1722 (2018).